This is a preproof accepted article for *Mineralogical Magazine*
This version may be subject to change during the production process
DOI: 10.1180/mgm.2025.10187

High temperature polymorphic transition and crystal structures of feldspar-related $SrZn_2P_2O_8$

Liudmila A. Gorelova[1*], Maria G. Krzhizhanovskaya[1], Valentina A. Yukhno[1], Olga Yu. Shorets[2], Irina A. Volkova[1], Oleg S. Vereshchagin[1]

Corresponding author: *l.gorelova@spbu.ru

[1] Saint Petersburg State University, Universitetskaya Emb. 7/9, 199034 St. Petersburg, Russia.

[2] Grebenshchikov Institute of Silicate Chemistry, Makarova Emb. 2, 199034 St. Petersburg, Russia

Abstract

Feldspars are among the most common phases in the Earth's crust and are characterized by wide variations in chemical composition and crystal structure motifs. In this paper, we synthesized $SrZn_2P_2O_8$ and studied it by means of scanning electron microscopy, electron microprobe analysis, powder X-ray diffraction at ambient and high-temperature (up to 900 ºC) conditions. We have structurally characterized for the first time layered triclinic β-modification of $SrZn_2P_2O_8$ (space group $P\bar{1}$, a = 5.0109(8), b = 8.6202(13), c = 9.7527(15) Å, α = 118.088(3), β = 74.622(6), γ = 87.525(6)°, V = 351.29(10) Å^3), which is structurally related to hexacelsian. The high-temperature study demonstrated that β-$SrZn_2P_2O_8$ irreversibly transformed into framework monoclinic paracelsian-like α-$SrZn_2P_2O_8$ (space group $P2_1/c$, a = 8.3163(2), b = 9.5023(2), c = 9.0248(2) Å, β = 92.285(1)°, V = 712.60(1) Å^3) above 600 °C, which, in turn, is stable up to 900 °C, when it melts. Though the crystal structures of α- and β-modification of $SrZn_2P_2O_8$ are different (framework and layered, respectively), their thermal expansion is similar: $\alpha_V \sim 26 \pm 1 \times 10^{-6}$ °C^{-1}, $\alpha_{max} / \alpha_{min} \sim 5$. The possible occurrence of the corresponding minerals in nature is discussed.

Keywords: feldspar; paracelsian; thermal expansion; phase transition; $SrZn_2P_2O_8$; metastable

1. Introduction

Feldspars are one of the most important groups of minerals, as they are widespread in the Earth's crust and were found in a number of celestial bodies (e.g., Wood *et al.*, 1970; Zolensky *et al.*, 2006; Jambon *et al.*, 2008; Chandra *et al.*, 2016; Arai and Maruyama, 2017; Knibbe, 2018). Traditionally (e.g., Ribbe, 1983; Back, 2022) feldspar group minerals includes natural compounds having three-dimensional (3D) framework of tetrahedra. This 3D framework is formed by corner-sharing tetrahedra and could have two topologies: feldspar and paracelsian (Smith and Brown, 1988). Krivovichev (2020) drew attention to the fact that minerals with MT_4O_8 general formula, where n is the average charge of the M cation (n = 1–2; M = Na, K, Rb, (NH_4), Ca, Sr, Ba) and k is the average charge of the T cation ($k = 4 - n/4$; T = Be, Zn, Al, B, Fe, Si, As, P), can have other topologies and suggest including them in feldspar family. According to this approach, feldspar family minerals crystallize in 5 different topologies. Four of them are TO_4-based (feldspar (3D), paracelsian (3D), svyatoslavite (3D) and dmisteinbergite (layered or 2D)) and one is TO_6-based (hollandite (3D)). According to this conception, feldspar family with general formula MT_4O_8 includes 31 mineral species. However, this classification was not approved by International Mineralogical Association (IMA) and contradicts Mills et al. (2009), who stated that "...mineral families apply to groups and/or supergroups having similar structural and/or chemical features that make them unique". Most probably, minerals belonging to feldspar family, suggested by Krivovichev (2020) should be divided into three separate groups, depending on their structural motif, i.e. framework (including feldspar, paracelsian and svyatoslavite topologies), layered (with dmisteinbergite topology) and TO_6-based (i.e. hollandite topology). For further discussion the minerals with dmisteinbergite topology, which include dmisteinbergite, hexacelsian, kokchetavite, cymrite, minjangite and recently discovered pfaffenbergite and wodegongenite will be named hexacelsian-type minerals.

There are also a number of synthetic compounds with general formula MT_4O_8. Most of them have feldspar or paracelsian topology, whereas the number of compounds with

https://doi.org/10.1180/mgm.2025.10187 Published online by Cambridge University Press

dmisteinbergite and svyatoslavite topology is relatively small (Czaya, 1972; Dollase; and Ross, 1993; David *et al.*, 2013; Dal Bo *et al.*, 2014; Pan *et al.*, 2017; Hwang *et al.*, 2023; Wang *et al.*, 2024). Interestingly, synthetic compound with general formula MT_4O_8, in which *T* site is occupied by P, Zn or Co could have topology not known in nature. Notably, two synthetic compounds (α-$CaZn_2P_2O_8$ (Jakeman and Cheetham, 1988) and $SrCo_2P_2O_8$ (El Bali *et al.*, 1993)) have triclinic (space group $P\bar{1}$) layered crystal structures similar to dmisteinbergite / hexacelsian, but not identical to them.

Only two synthetic strontium zinc phosphate are known: $SrZn_2P_2O_8$ (Hemon and Courbion, 1990) and $SrZnP_2O_7$ (Yuan *et al.*, 2007). The well characterized $SrZn_2P_2O_8$ with feldspar-related stoichiometry crystallizes in monoclinic (space group $P2_1/c$) symmetry with paracelsian topology. There are also data on the existence of its metastable high-temperature modification, named β-$SrZn_2P_2O_8$ (Sarver *et al.*, 1961). However, this modification was not structurally characterized and was obtained in conditions that are unattainable today (by rapid cooling in mercury). Though zinc phosphates are not very widespread in nature, to date about 50 minerals with essential P, Zn and O are known.

Here, the thermal behavior of $SrZn_2P_2O_8$ is described in detail with the focus on formation of different polymorphic modification and their thermal expansion. Besides, assumptions have been made about the possibility of finding related minerals in nature.

2. Materials and methods

2.1. Synthesis and primary characterization

The α-$SrZn_2P_2O_8$ has been synthesized using solid-state reactions method from chemically pure $SrCO_3$ (99.99%, Sigma-Aldrich), ZnO (99.99%, Sigma-Aldrich), $NH_4H_2PO_4$ (99.99%, Sigma-Aldrich) taken in stoichiometric ratios. The reagent mixtures were thoroughly ground in an agate mortar, pressed into pellets, and transferred to platinum crucibles. Crucibles were placed into a muffle furnace and sequentially heated in air at 400 °C for 6 h and at 900 °C for 36 h. The polymorphic transformations of $SrZn_2P_2O_8$ have been studied by solid-state

https://doi.org/10.1180/mgm.2025.10187 Published online by Cambridge University Press

reactions and melt crystallization method in the temperature range from 800 to 1200 °C for 0.5–24 hours.

The phase composition of obtained samples was controlled by powder X-ray diffraction (PXRD) using a MiniFlex II (Rigaku Oxford Diffraction, Japan) diffractometer ($CuK\alpha_{12}$ radiation, 30 kV / 15 mA, Bragg-Brentano geometry, PSD D-Tex Ultra detector). The chemical composition of the obtained compounds was controlled using a S-3400N (Hitachi, Japan) scanning electron microscope (SEM) equipped with AzTec Energy 350 energy dispersive (EDX) spectrometer (Oxford Diffraction, UK).

2.2. High-temperature powder X-ray diffraction study

High-temperature (HT) behavior of $SrZn_2P_2O_8$ has been studied under heating in air by HT powder X-ray diffraction (PXRD) using an Ultima IV (Rigaku, Japan) diffractometer ($CuK\alpha_{12}$ radiation, 40 kV / 30 mA, Bragg-Brentano geometry, PSD D-Tex Ultra detector, goniometer radius = 185 mm) with a thermo-attachment in the range of 30–900 °C, with the temperature steps of 30 °C. The fine-powdered sample was deposited on a platinum sample holder (20 × 12 × 1.5 mm) from an ethanol suspension (Filatov, 1971). An external Si standard was used before the measurements to control the 2θ correctness. The calculations of the unit-cell parameters were performed using the program package Topas 5.0 (Bruker, 2014; Dinnebier *et al.*, 2019). The temperature dependence of the unit-cell parameters was described by linear and / or quadratic polynomial functions, depending on the amount of the experimental points. The calculation and visualization of the thermal expansion parameters tensor was performed using the TTT program package (Bubnova *et al.*, 2013).

2.3. Crystal structure refinement

The crystal structure of β-$SrZn_2P_2O_8$ was refined using Rietveld refinement method with the use of the Bruker TOPAS 5.0 software package (Bruker, 2014; Dinnebier *et al.*, 2019). A PXRD pattern was obtained with an Ultima IV (Rigaku, Japan) diffractometer ($CuK\alpha_{12}$ radiation, 40 kV / 30 mA, Bragg-Brentano geometry, PSD D-Tex Ultra detector, goniometer radius = 285

https://doi.org/10.1180/mgm.2025.10187 Published online by Cambridge University Press

mm). The powder XRD plot was collected in the range 5–100° 2θ at ambient temperature. The collecting time was about 14 h. The structure model of triclinic $SrCo_2P_2O_8$ (El Bali *et al.*, 1993) was used as starting models for the structure refinement. The peak profile was modeled using the Thompson-Cox-Hastings pseudo-Voigt function (TCHZ). Atomic coordinates were refined for all atomic positions (see Table S1 and CIF file). Isotropic atomic displacement parameters B_{iso} were used for all the atoms; B_{iso} were constrained for the groups of atoms (Sr, Zn1–2, P1–2, O1–8) and then refined free of limits. Soft restraints for all P–O bonds in tetrahedra as well as selected distances and angles in zinc polyhedra were realized using Topas 5.0 Launch mode with the weighting factor for penalties K = 3. The correctness of the refined structure was confirmed by low values of final agreement factors (Table 1). The observed and calculated powder X-ray diffraction patterns (final Rietveld refinement plot) are shown in Figure 1. Atomic coordinates and displacement parameters are given in CIF file (Supplementary material) and selected interatomic distances are shown in Table 2. The calculated quantity of the impurity phase modelled by the crystal structure of a trigonal $CaZn_2P_2O_7$ (Czaya, 1972) was about 3 wt. %

3. Results and discussion

3.1. Formation conditions of different polymorphs of $SrZn_2P_2O_8$

The single-phase sample of α-$SrZn_2P_2O_8$ (space group $P2_1/c$, a = 8.3163(2), b = 9.5023(2), c = 9.0248(2) Å, β = 92.285(1)°, V = 712.60(1) Å^3) has been obtained using solid-state reactions method at 900 °C for 36 h. We were unable to obtain well-cut crystals, but studies of the melt particles revealed a stepped surface relief and perfect cleavage (Figure S1a). The compound is chemically homogeneous, free of impurities and is characterized by a predetermined elemental ratio (Sr:Zn:P:O 1:2:2:8; Figure S1b). All the attempts to synthesize its high-temperature modification using solid state reactions and melt crystallization methods with different heat or cooling rate and time of heat treatment were unsuccessful. Nevertheless this polymorphic modification has been obtained during the HT PXRD experiment. The α-$SrZn_2P_2O_8$ modification has been quickly heated in air up to 900 °C with the intermediate annealing at 300

https://doi.org/10.1180/mgm.2025.10187 Published online by Cambridge University Press

and 600 °C. Above 900 °C the sample melted and the further heating was carried out at a rate of 5 °C/min up to 1200 °C with the annealing each 30 °C for about 30 minutes. After that the sample has been rapidly cooled to ambient temperature. As a result β-$SrZn_2P_2O_8$ was obtained. The exact reasons for the formation of this phase during the HT PXRD experiment are unclear. As with other metastable phases, we are inclined to consider kinetic causes (long heating, rapid quenching) and crystallization from a superheated (boiling) melt, in which unusual atomic polymerization could exist (e.g., Toda *et al.*, 2021).

Previously, α-$SrZn_2P_2O_8$ doped by different cations has been obtained by different methods (chloride-flux method, solid state reactions etc.) at the temperature from 550 to 1000 °C, depending on the admixtures (Hemon and Courbion, 1990; Yang and Chen, 2006; Yi *et al.*, 2010; Li *et al.*, 2014; Guo *et al.*, 2016; Khidhirbrahmendra *et al.*, 2019; Xu *et al.*, 2020). The existence of high-temperature β-$SrZn_2P_2O_8$ has been previously mentioned only once by Sarver et al. (1961). According to their data the high-temperature polymorph existences between 1035 and 1175 °C, when it melts (above 1175 °C). They also mentioned that this phase can be quenched at ambient temperature using only extremely rapid cooling by pouring a melted batch into liquid Hg, water or over dry ice, whereas the cooling in air always results in the formation of α-$SrZn_2P_2O_8$. However, the authors were unable to obtain any crystallographic data on β-$SrZn_2P_2O_8$.

The stable α-$SrZn_2P_2O_8$ is structurally related to feldspar compounds with paracelsian topology (Figure 2a, b) and has many structural analogues with different chemical composition (e.g. alumino-, borosilicates, beryllium phosphates, etc.). As far as we know its high-temperature β-modification, has only two direct structural analogues, namely $SrCo_2P_2O_8$ (El Bali *et al.*, 1993) and α-$CaZn_2P_2O_8$ (Jakeman and Cheetham, 1988). However, it could be also considered as hexacelsian-type compound (see below). $SrCo_2P_2O_8$ has been obtained by slow cooling (10 °C/h) of the melt (obtained at 1200 °C) with stoichiometric composition (El Bali *et al.*, 1993). The synthesis of α-$CaZn_2P_2O_8$ is completely different (Jakeman and Cheetham, 1988): the

https://doi.org/10.1180/mgm.2025.10187 Published online by Cambridge University Press

polycrystalline sample was prepared in two steps (1) dissolving of $CaCO_3$, ZnO and $NH_4H_2PO_4$ in acid solution; (2) the dried powder was ground and fired at 800 °C for 24 h. The single crystals of α-$CaZn_2P_2O_8$ were grown using $ZnCl_2$ as a flux, but Jakeman and Cheetham (1988) did not provide the temperature and speed of their crystallization. It should be also noted that similar triclinic crystal structure can be also obtained with Mg admixture ($CaZn_{2-x}Mg_xP_2O_8$, x = 0–0.75), but pure Mg analogue cannot be obtained (Jakeman and Cheetham, 1988). It is interesting to note that anhydrous calcium and magnesium phosphates are represented by only two minerals (keplerite and stanfieldite), both of which have been discovered in native Fe-rich meteorites (Britvin *et al.*, 2020, 2021). Thus, it can be assumed that reducing conditions are important for the occurrence of such phosphates in nature.

3.2. Crystal structure of β-$SrZn_2P_2O_8$

No crystallographic data were previously available for β-$SrZn_2P_2O_8$ (Sarver *et al.*, 1961). According to our data, the crystal structure of β-$SrZn_2P_2O_8$ (space group $P\bar{1}$, a = 5.0109(8), b = 8.6202(13), c = 9.7527(15) Å, α = 118.088(3), β = 74.622(6), γ = 87.525(6)°, V = 351.29(10) Å^3) can be described as layered structure (Figure 2c), consisting of PO_4, ZnO_4 tetrahedra. $Zn2O_4$ tetrahedra are connected to each other *via* corners, whereas $Zn1O_4$ tetrahedra are connected to each other along edges. This type of tetrahedra connection is not common for Zn, but it is known in some crystal structures (e.g. Ghose *et al*., 1977; Wiebcke, 2002; Harrisson, 2010). Thus the ZnO_4 tetrahedra form Zn_4O_{12} structural units (Figure 3a). These units form layers connecting *via* PO_4 tetrahedra (Figure 2c, 4a). The resulted layers are formed by three-, four- and six-membered rings. The interlayer space is occupied by Sr atoms in eight-fold coordination. SrO_8 polyhedra are connected to each other through the vertices and edges and form the chains along the *a* axis (Figure 3b).

The crystal structures of most closely related compounds, i.e. triclinic modifications of $SrCo_2P_2O_8$ and $CaZn_2P_2O_8$, are usually described, as consisting of PO_4 and $Co2O_4$ / $Zn2O_4$ tetrahedra and $Co1O_5$ / $Zn1O_5$ distorted trigonal bipyramids with four bonds about 1.94–2.04 Å

https://doi.org/10.1180/mgm.2025.10187 Published online by Cambridge University Press

and the fifth bond 2.45 and 2.52 for Co and Zn, respectively. Although the necessity of the existence of a fifth long bond seems doubtful, the additional bond has to be included in the coordination sphere of Co / Zn atoms according to the bond length analysis (Jakeman and Cheetham, 1988). In case of β-$SrZn_2P_2O_8$ the fifth Zn–O bond is longer than 2.7 Å, whereas four other bonds are in the range of 1.81–2.23 Å. To understand whether it is necessary to include the fifth oxygen atom in the coordination sphere of Zn, the bond weights (BW) for this cation were calculated (Table S2). The obtained results demonstrate that in case of $SrCo_2P_2O_8$ and $CaZn_2P_2O_8$ the BW of the fifth Co1–O7 and Zn2–O8 bond are 0.0938 and 0.0361, respectively, i.e. an order of magnitude lower than for other four bonds. The BW for Zn1–O7 in β-$SrZn_2P_2O_8$ is still an order of magnitude lower (0.0011), i.e. including this bond in the coordination sphere of Zn1 is not advisable.

Generally all these three compounds (β-$SrZn_2P_2O_8$, $SrCo_2P_2O_8$ and α-$CaZn_2P_2O_8$) with layered triclinic crystal structures have similarities with hexacelsian-type minerals. The main difference being that in hexacelsian-type minerals TO_4 tetrahedra are joined to each other *via* corners, whereas some of *T* atoms in crystal structures of β-$SrZn_2P_2O_8$, $SrCo_2P_2O_8$ and α-$CaZn_2P_2O_8$ are connected to each other *via* edges. Most probably, this difference leads to a decrease of symmetry in crystal structure of β-$SrZn_2P_2O_8$, $SrCo_2P_2O_8$ and α-$CaZn_2P_2O_8$ to triclinic. Nevertheless layers consist of six-membered rings of TO_n polyhedra (Figure 4) in all types of crystal structures. In all cases the *M* cations are located in the interlayer space.

It is interesting to note that both $SrCo_2P_2O_8$ and $CaZn_2P_2O_8$ do not form framework crystal structures with paracelsian topology unlike $SrZn_2P_2O_8$. $SrCo_2P_2O_8$ crystallizes only in triclinic (space group $P\bar{1}$) symmetry (El Bali *et al.*, 1993) with layered crystal structure, whereas $CaZn_2P_2O_8$ has triclinic (space group $P\bar{1}$; α-$CaZn_2P_2O_8$) and hexagonal (space group $P\bar{3}$; β-$CaZn_2P_2O_8$) polymorphs (Czaya, 1972; Jakeman and Cheetham, 1988), but both of them are layered too. A number of closely related compounds also do not exhibit similar polymorphism. Thus, $BaZn_2P_2O_8$ crystallizes only in monoclinic symmetry (space group $P2_1/c$) with framework

https://doi.org/10.1180/mgm.2025.10187 Published online by Cambridge University Press

paracelsian topology (Lucas *et al.*, 1998). $CaCo_2P_2O_8$ and $BaCo_2P_2O_8$ form completely different crystal structures (Faza *et al.*, 1950; Bircsak and Harrison, 1998; David *et al.*, 2013). We can assume that the key to polymorphism is not only the density of oxygen layers (as was suggested earlier), but also the fundamentally different thermal behaviour of large cations (e.g., Ca (R = 1.00 Å), Sr (R = 1.18 Å), Ba (R = 1.42 Å); Shannon, 1976), that lead to the limited isomorphism and changes in their coordination polyhedra.

3.3. Temperature behavior of different polymorphs of $SrZn_2P_2O_8$

According to the HT PXRD data, α-$SrZn_2P_2O_8$ is stable up to 900 °C, above which it starts to melt, whereas β-$SrZn_2P_2O_8$ is less stable and transforms into α-modification above 630 °C (Figure 5).

The temperature dependencies for the unit-cell parameters of both $SrZn_2P_2O_8$ modifications are shown in Figure 6. The volume thermal expansion of framework α-$SrZn_2P_2O_8$ equals 25 × 10^{-6} °C^{-1} that is close to the average volume expansion coefficient (α_V = 23 × 10^{-6} °C^{-1}) for different compounds with paracelsian topology (Gorelova *et al.*, 2023a). The thermal expansion of α-modification has sharply anisotropic character (α_{max} / α_{min} = 4.9) with the maximal expansion close to the *a* axis and minimal along *b* axis (Table 4, Figures 2a, 2b and 6a). It should be noted that though the anisotropic expansion is typical for paracelsian-like phases, the directions of maximal and minimal expansion are usually in the plane of the layer formed by four- and eight-membered rings of TO_4 tetrahedra (T = Si, Al, B). In case of α-$SrZn_2P_2O_8$ the direction of maximal expansion is perpendicular to these layers and is located along the flexible crankshaft chains of TO_4 tetrahedra (T = Zn, P), that is more typical for compounds with feldspar topology. The similar behavior has been previously described for $BaAs_2Zn_2O_8 \cdot H_2O$ (Gorelova *et al.*, 2022).

The layered β-$SrZn_2P_2O_8$ shows very similar thermal behavior despite a different structural motif. Its volume expansion and degree of anisotropy are slightly large (α_V = 27 × 10^{-6} °C^{-1}; α_{max} / α_{min} = 5.6). The direction of maximal thermal expansion practically coincides with

https://doi.org/10.1180/mgm.2025.10187 Published online by Cambridge University Press

the *c* axis, i.e. it is perpendicular to the layer plane (Table 4, Figures 2c and 6b) that is generally typical for layered crystal structures. Additionally, such a sharp expansion along *c* axis can be due to the so-called "preparing" of the crystal structure to a phase transition into α-modification. The thermal expansion within the layer plane is quite anisotropic too (α_{11} / α_{22} = 4.1), that can be explained by the low symmetry of the studied compound, for which the shear character of thermal deformations is typical (Filatov, 1990, 2011).

3.4. Possible natural formation conditions

According to the International Mineralogical Association (IMA) List of Minerals, 47 minerals contain essential Zn, P and O, while only two of them are anhydrous, namely kuksite $Pb_3Zn_3TeO_6(PO_4)_2$ (Kim *et al.*, 1990) and tululite $Ca_{14}(Fe^{3+},Al)(Al,Zn,Fe^{3+},Si,P,Mn,Mg)_{15}O_{36}$ (or $Ca_{14}(Fe^{3+}O_6)[(Si,P)O_4][(Al,Zn)_7O_{13}]$; Khoury *et al.*, 2016). Kuksite was found in several Au, Ag-related deposits in Russia (Kim *et al.*, 1990; Kondratieva *et al.*, 2021) and the USA (e.g., Kampf *et al.*, 2009, 2022; Mills *et al.*, 2010; Yang *et al.*, 2021) and is always formed as secondary mineral at low temperatures (below 250 °C), whereas its synthetic analogue has been prepared above 500 °C by solid-state methods (Mill', 2009b; a). Tululite is found in combustion metamorphic rocks in central Jordan only (Khoury *et al.*, 2016; Sokol *et al.*, 2020; Galuskina *et al.*, 2021) and is formed at about 800–850 °C and ambient pressures.

There is no a single mineral with essential Zn, P and O, which contain Sr^{2+} or Ba^{2+}. Besides, only 11 mineral with essential Zn, P and O contain Ca^{2+} and only 5 of them contain Pb^{2+}. Among calcium minerals are: batagayite $CaZn_2(Zn,Cu)_6(PO_4)_4[PO_3(OH)]_3\cdot 12H_2O$ (Yakovenchuk *et al.*, 2018), ehrleite $Ca_2ZnBe(PO_4)_2(PO_3OH)\cdot 4H_2O$ (Robinson *et al.*, 1985), falsterite $Ca_2MgMn^{2+}{}_2Fe^{2+}{}_2Fe^{3+}{}_2Zn_4(PO_4)_8(OH)_4(H_2O)_{14}$ (Kampf *et al.*, 2012), guimaraesite $Ca_2Be_4Zn_5(PO_4)_6(OH)_4\cdot 6H_2O$ (Chukanov *et al.*, 2008), hillite $Ca_2Zn(PO_4)_2\cdot 2H_2O$ (Yakubovich *et al.*, 2003), jahnsite-(CaMnZn) $CaMn^{2+}Zn_2Fe^{3+}{}_2(PO_4)_4(OH)_2\cdot 8H_2O$ (Grey *et al.*, 2020), jungite $Ca_2Zn_4Fe^{3+}{}_8(PO_4)_9(OH)_9\cdot 16H_2O$ (Moore and Ito, 1980), scholzite and parascholzite $CaZn_2(PO_4)_2\cdot 2H_2O$ (Strunz, 1948; Strunz and Tennyson, 1956; Sturman *et al.*, 1981),

https://doi.org/10.1180/mgm.2025.10187 Published online by Cambridge University Press

skorpionite $Ca_3Zn_2(PO_4)_2(CO_3)(OH)_2 \cdot H_2O$ (Krause *et al.*, 2008) and already mentioned above tululite. Among led minerals are: cuprodongchuanite $Pb_4CuZn_2(PO_4)_4(OH)_2$ (Sun *et al.*, 2021), cuprozheshengite $Pb_4CuZn_2(AsO_4)_2(PO_4)_2(OH)_2$ (Sun *et al.*, 2024a), dongchuanite $Pb_4ZnZn_2(PO_4)_4(OH)_2$ (Li *et al.*, 2023), zheshengite $Pb_4ZnZn_2(AsO_4)_2(PO_4)_2(OH)_2$ (Sun *et al.*, 2024b) and mentioned above kuksite. It is interesting to note that all the Pb-dominant minerals except kuksite were discovered recently, have supergene origin (low temperatures, low pressures) and are members of the dongchuanite group (Sun *et al.*, 2024a; 2024b). The Ca-dominant minerals are extremely rare and most of them (except sholzite and parasholzite) are found in 1-2 localities (mindat.org, Ralph *et al.*, 2025). Notably all these minerals are secondary low-temperature minerals.

It should be noted that none of the mentioned minerals contain Sr even in trace amount, although Sr is usually dispersed in calcium minerals (e.g., apatite group minerals; Pekov *et al.*, 1996). Besides Sr-containing minerals rarely have layered structures (exceptions are lamprophyllite and Sr-rich borates; e.g., Pekov *et al.*, 2004; Pekov, 2005; Ralph *et al.*, 2025). It is the structural motif of these minerals that may explain the absence of calcium (see below).

The crystal structures of the minerals, mentioned above, can be formed by different combinations of Zn- and P-based polyhedra: phosphorous is always surrounded by four O atoms, whereas Zn can be coordinated by 4 and / or 6 oxygen atoms. The crystal structures of kuksite, tululite, ehrleite, falsterite, skorpionite, scholzite and parasholzite are based on layers of corner-sharing ZnO_4 and PO_4 tetrahedra (Taxer, 1975; Hawthorne and Grice, 1987; Taxer and Bartl, 1997; Krause *et al.*, 2008; Mills *et al.*, 2010; Kampf *et al.*, 2012; Khoury *et al.*, 2016; Tobase *et al.*, 2019). In crystal structures of guimaraesite, hillite and jahnsite-(CaMnZn) phosphorous is coordinated by 4 oxygen atoms, whereas Zn is coordinated by six oxygens (Yakubovich *et al.*, 2003; Chukanov *et al.*, 2008; Grey *et al.*, 2020). Pb-dominant minerals, related to dongchuanite group, have layered crystal structure. The layers are formed by TO_4 (T = Zn, P, As) tetrahedra and XO_6 octahedra (X = Zn, Cu), i.e. in their crystal structures Zn is surrounded by four and six

https://doi.org/10.1180/mgm.2025.10187 Published online by Cambridge University Press

oxygen atoms (Sun *et al.*, 2024a; b). The similar tendency is in the crystal structure of batagayite, which layers are formed by PO_4 and ZnO_4 tetrahedra and TO_6 (T = Zn, Cu, Mg) octahedra (Yakovenchuk *et al.*, 2018).

Nevertheless, to date three Sr-dominant minerals are known in feldspar family, namely slawsonite $SrAl_2Si_2O_8$ (Griffen *et al.*, 1997), pekovite $SrB_2Si_2O_8$ (Pautov *et al.*, 2004) and strontiohurlbutite $SrBe_2P_2O_8$ (Rao *et al.*, 2014). All of them belong to the paracelsian topology, i.e. have framework crystal structures. The interesting fact is that pekovite has both Ca- and Ba-dominant analogues, namely danburite (Phillips *et al.*, 1974) and maleevite (Pautov *et al.*, 2004), whereas slawsonite has only Ba-dominant analogue, namely paracelsian (Smith, 1953) and strontiohurlbutite has only Ca-dominant analogue, namely hurlbutite (Lindbloom *et al.*, 1974). Notably, minerals with the composition of $CaAl_2Si_2O_8$ and $BaBe_2P_2O_8$ are known in nature, but crystallize in other topologies. $CaAl_2Si_2O_8$ is known in feldspar (anorthite; Wainwright and Starkey, 1971), dmisteinbergite (dmisteinbergite; Chesnokov *et al.*, 1990; Zolotarev *et al.*, 2019), svyatoslavite (svyatoslavite; Chesnokov *et al.*, 1989; Krivovivhev *et al.*, 2012) and hollandite (stoefflerite; Tschauner and Ma, 2017) topologies. $BaBe_2P_2O_8$ is known in dmisteinbergite topology only (minjangite; Rao *et al.*, 2015). The recent discover of two new hexacelsian-type metastable minerals of feldspar family, namely pfaffenbergite $KNa_3(Al_4Si_{12})O_{32}$ (Silvio *et al.*, 2025) and wodegongjieite $KCa_3(Al_7Si_9)O_{32}$ (Mugnaioli *et al.*, 2022), is one more confirmation that layered modification of $SrZn_2P_2O_8$ can be also found in nature.

Based on that we assume that the zinc phosphate minerals with both feldspar- and hexacelsain-type crystal structures (i.e. different polymorphic modifications of $SrZn_2P_2O_8$ or $CaZn_2P_2O_8$), can be found in nature. The α-modification of $SrZn_2P_2O_8$ phase with the paracelsian structure may be found in nature under high-temperature and low-pressure conditions. However, the existence of β-modification of $SrZn_2P_2O_8$ is questionable, as this phase is undoubtedly metastable and requires very specific formation conditions (e.g., superheated melt).

https://doi.org/10.1180/mgm.2025.10187 Published online by Cambridge University Press

4. Conclusion

During this work, the crystal structure of β-$SrZn_2P_2O_8$ was determined for the first time. It has been shown that β-$SrZn_2P_2O_8$ can be synthesized by the rapid cooling of stoichiometric $SrZn_2P_2O_8$ melt in air. According to the obtained results, the triclinic (space group $P\bar{1}$) crystal structure of β-$SrZn_2P_2O_8$ is layered and close to $SrCo_2P_2O_8$ and α-$CaZn_2P_2O_8$. The β-$SrZn_2P_2O_8$ transforms into stable α-modification with framework crystal structure of paracelsian topology when heated above 630 °C. The thermal expansion coefficients of both $SrZn_2P_2O_8$ modifications were determined. The volume expansion ($\alpha_V = 26 \pm 1 \times 10^{-6}$ °C^{-1}) and the anisotropy of thermal expansion are similar for both phases despite that they have significantly different structures. We assume the possibility of discovering a new feldspar- and hexacelsain-type minerals in nature.

Acknowledgments: The authors are grateful to anonymous reviewers for a careful examination of the manuscript contents and positive feedback. The authors express their gratitude to Principal editor Stuart Mills and Associate editor Irina Galuskina for editorial handing of this contribution. The authors thank X-ray Diffraction Centre and Geomodel Centre of Saint Petersburg State University for providing instrumental and computational resources. This research was funded by the Russian Science Foundation, grant number 22-77-10033.

Competing interests: The authors declare none.

References

Arai, T. and Maruyama, S. (2017) Formation of anorthosite on the Moon through magma ocean fractional crystallization. *Geoscience Frontiers*, **8**, 299–308. Elsevier Ltd.

Back, M.E. (2022) *Fleischer's Glossary of Mineral Species*. P. in.: Mineralogical Association of Canada, Quebec, Canada, 431 pp.

El Bali, B., Boukhari, A., Holt, E.M. and Aride, J. (1993) Strontium dicobalt orthophosphate. *Journal of Crystallographic and Spectroscopic Research*, **23**, 1001–1004.

https://doi.org/10.1180/mgm.2025.10187 Published online by Cambridge University Press

Bircsak, Z. and Harrison, W.T.A. (1998) Barium cobalt phosphate, $BaCo_2(PO_4)_2$. *Acta Crystallographica Section C: Crystal Structure Communications*, **54**, 1554–1556. International Union of Crystallography.

Britvin, S.N., Krzhizhanovskaya, M.G., Bocharov, V.N. and Obolonskaya, E. V. (2020) Crystal Chemistry of Stanfieldite, $Ca_7M_2Mg_9(PO_4)_{12}$ (M = Ca, Mg, Fe^{2+}), a Structural Base of $Ca_3Mg_3(PO_4)_4$ Phosphors. *Crystals*, **10**, 1–14.

Britvin, S.N., Galuskina, I.O., Vlasenko, N.S., Vereshchagin, O.S., Bocharov, V.N., Krzhizhanovskaya, M.G., Shilovskikh, V. V., Galuskin, E. V., Vapnik, Y. and Obolonskaya, E. V. (2021) Keplerite, $Ca_9(Ca_{0.5}\square_{0.5})Mg(PO_4)_7$, a new meteoritic and terrestrial phosphate isomorphous with merrillite, $Ca_9NaMg(PO_4)_7$. *American Mineralogist*, **106**, 1917–1927.

Bruker, A. (2014) *Topas 5.0, General Profile and Structure Analysis Software for Powder Diffraction Data*. P. in.: Karlsruhe, Germany.

Bubnova, R.S., Firsova, V.A. and Filatov, S.K. (2013) Software for determining the thermal expansion tensor and the graphic representation of its characteristic surface (Theta to Tensor-TTT). *Glass Physics and Chemistry*, **39**, 347–350.

Chandra, U., Pandey, K.K., Parthasarathy, G. and Sharma, S.M. (2016) High-pressure investigations on Piplia Kalan eucrite meteorite using in-situ X-ray diffraction and ^{57}Fe Mössbauer spectroscopic technique up to 16 GPa. *Geoscience Frontiers*, **7**, 265–271. Elsevier Ltd.

Chesnokov, B.V., Lotova, E.V., Pavlyuchenko, V.S., Nigmatulina, E.N., Usova, L.V., Bushmakin, A.R. and Nishanbaev, T.P. (1989) Svyatoslavite, $CaAl_2Si_2O_8$ (orthorhombic), a new mineral. *Zap. Vses. Mineral. Obshch.*, **118**, 111–114 (in Russian).

https://doi.org/10.1180/mgm.2025.10187 Published online by Cambridge University Press

Chesnokov, B.V., Lotova, E.V., Nigmatulina, E.N., Pavlyuchenko, V.S. and Bushmakin, A.F. (1990) Dmisteinbergite $CaAl_2Si_2O_8$ (hexagonal) - A new mineral. *Zap. Vses. Mineral. Obshch.*, **119**, 43–45 (in Russian).

Chukanov, N. V, Atencio, D., Zadov, A.E., Filho, L.A.D.M. and Coutinho, J.M.V. (2008) Guimarãesite, a new Zn-dominant monoclinic roscherite-group mineral from Itinga, Minas Gerais, Brazil. *New Data on Minerals*, **42**, 11–15.

Czaya, R. (1972) Dehydration and transformation phases of scholzite $CaZn_2(PO_4)_2.2H_2O$. *Acta Crystallographica Section B Structural Crystallography and Crystal Chemistry*, **28**, 322–323. International Union of Crystallography.

Dal Bo, F., Hatert, F. and Baijot, M. (2014) Crystal chemistry of synthetic $M^{2+}Be_2P_2O_8$ (M^{2+}= Ca, Sr, Pb, Ba) beryllophosphates. *The Canadian Mineralogist*, **52**, 337–350.

David, R., Kabbour, H., Pautrat, A. and Mentré, O. (2013) Puzzling polymorphism of layered $Ba(CoPO_4)_2$. *Inorganic Chemistry*, **52**, 8732–8737.

Dinnebier, R.E., Leineweber, A. and Evans, J.S.O. (2019) *Rietveld Refinement: Practical Powder Diffraction Pattern Analysis using TOPAS*. P. in.: De Gruyter, Berlin, Boston, 331 pp.

Dollase;, W.A. and Ross, C.R. (1993) Crystal structures of the body-centered tetragonal tectosilicates: $K_{1.14}Mg_{0.57}Si_{1.43}O_4$, $K_{1.10}Zn_{0.55}Si_{1.45}O_4$, and $K_{1.11}Fe^3{}_{1.11}Si_{0.89}O_4$. *American Mineralogist*, **78**, 627–632.

Faza, N., Treutmann, W. and Babel, D. (1950) Struktur- und magnetochemische Untersuchungen an den ternaeren Phosphaten $Ba_2M(II)(PO_4)_2$ (M(II) = Mn, Co) und Strukturverfeinerung von $BaNi_2(PO_4)2$. *Zeitschrift fuer Anorganische und Allgemeine Chemie*, 627–692 [in German].

https://doi.org/10.1180/mgm.2025.10187 Published online by Cambridge University Press

Filatov, S.K. (1971) Anomale Wärmeausdehnung von V_2O_5. *Crystal Research and Technology*, **6**, 777-785 [in German].

Filatov, S.K. (1990) *Vysokotemperaturnaya Kristallokhimiya. Teoriya, metody i rezul'taty issledovanii; (High-temperature crystal chemistry: Theory, methods and results of investigations)*. P. in.: Nedra: Leningrad, Russia, 289 pp [in Russian].

Filatov, S.K. (2011) General concept of increasing crystal symmetry with an increase in temperature. *Crystallography Reports*, **56**, 953–961.

Galuskina, I.O., Stachowicz, M., Woźniak, K., Vapnik, Y. and Galuskin, E. (2021) Mcconnellite, $CuCrO_2$ and ellinaite, $CaCr_2O_4$, from varicoloured spurrite marble of the Daba-Siwaqa area, Hatrurim Complex, Jordan. *Mineralogical Magazine*, **85**, 387–397. Cambridge University Press.

Ghose, S., Boving, P., LaChapelle, W.A. and Wan C. (1977) Reinerite, $Zn_3(AsO_3)_2$; an arsenite with a novel type of Zn-tetrahedral double chain. *American Mineralogist*, **62**, 1129–1134.

Gorelova, L., Khandarkhaeva, S., Yukhno, V., Krzhizhanovskaya, M., Vereshchagin, O. and Dubrovinsky, L.S. (2023a) Topologically prone or cation compression restricted phase transition: An example of feldspar-related $SrGe_2B_2O_8$. *Journal of Alloys and Compounds*, **938**, 168642.

Gorelova, L.A., Pakhomova, A.S., Krzhizhanovskaya, M.G., Winkler, B., Krivovichev, S. V. and Dubrovinsky, L.S. (2020) Pressure-Induced Phase Transitions in Danburite-Type Borosilicates. *Journal of Physical Chemistry C*, **124**, 26048–26061.

Gorelova, L.A., Vereshchagin, O.S., Bocharov, V.N., Pankin, D. V. and Đorđević, T. (2022) Temperature-Induced Phase Transition in a Feldspar-Related Compound $BaZn_2As_2O_8{\cdot}H_2O$. *Minerals*, **12**, 1262.

https://doi.org/10.1180/mgm.2025.10187 Published online by Cambridge University Press

Gorelova, L.A., Vereshchagin, O.S., Bocharov, V.N., Krivovichev, S. V., Zolotarev, A.A. and Rassomakhin, M.A. (2023b) $CaAl_2Si_2O_8$ polymorphs: sensitive geothermometers and geospeedometers. *Geoscience Frontiers*, **14**, 101458. China University of Geosciences (Beijing).

Grey, I.E., Keck, E., Kampf, A.R., MacRae, C.M., Cashion, J.D. and Glenn, A.M. (2020) Jahnsite-(CaMnZn) from the Hagendorf-Süd pegmatite, Oberpfalz, Bavaria, and structural flexibility of jahnsite-group minerals. *Mineralogical Magazine*, **84**, 547–553.

Griffen, D.T., Ribbe, P.H. and Gibbs, G.V. (1977) The structure of slawsonite, a strontium analog of paracelsian. *American Mineralogist*, **62**, 31–35.

Guo, T., Li, Y., Wahyudi, O., Chen, S., Wang, X. and Chen, J. (2016) Microwave Dielectric Properties of $AZn_2(PO_4)_2$ (*A* = Sr, Ba) Ceramics. *Ferroelectrics*, **492**, 91–102.

Harrison, W.T. (2010) β-$Zn_3(AsO_3)_2$. *Acta Crystallographica C*, **66**, 64–66.

Hawthorne, F.C. and Grice, J.D. (1987) The crystal structure of ehrleite, a tetrahedral sheet structure. *The Canadian Mineralogist*, **25**, 767–774.

Hemon, A. and Courbion, G. (1990) The crystal structure of α-$SrZn_2(PO_4)_2$: A hurlbutite type. *Journal of Solid State Chemistry*, **85**, 164–168.

Hwang, H., Seoung, D., Gatta, G.D., Blom, D.A., Vogt, T. and Lee, Y. (2023) Topotactic and reconstructive changes at high pressures and temperatures from Cs-natrolite to Cs-hexacelsian. *American Mineralogist*, **100**, 1562–1567.

Jakeman, R.J.B. and Cheetham, A.K. (1988) Combined Single-Crystal X-ray Diffraction and Magic Angle Spinning NMR Study of α-$CaZn_2(PO_4)_2$. *Journal of the American Chemical Society*, **110**, 1140–1143.

https://doi.org/10.1180/mgm.2025.10187 Published online by Cambridge University Press

Jambon, A., Boudouma, O., Fonteilles, M., Guillou, C.L.E., Badia, D. and Barrat, J.A. (2008) Petrology and mineralogy of the angrite Northwest Africa 1670. *Meteoritics and Planetary Science*, **43**, 1783–1795.

Kampf, A.R., Rossman, G.R. and Housley, R.M. (2009) Plumbophyllite, a new species from the blue bell claims near baker, San Bernardino County, California. *American Mineralogist*, **94**, 1198–1204.

Kampf, A.R., Mills, S.J., Simmons, W.B., Nizamoff, J.W. and Whitmore, R.W. (2012) Falsterite, $Ca_2MgMn^{2+}{}_2(Fe^{2+}{}_{0.5}Fe^{3+}{}_{0.5})_4Zn_4(PO_4)_8(OH)_4(H_2O)_{14}$, a new secondary phosphate mineral from the Palermo No. 1 pegmatite, North Groton, New Hampshire. *American Mineralogist*, **97**, 496–502.

Kampf, A.R., Missen, O.P., Mills, S.J., Ma, C., Housley, R.M., Chorazewicz, M., Marty, J., Coolbaugh, M. and Momma, K. (2022) Matthiasweilite, $PbTe^{4+}O_3$, a New Tellurite Mineral from the Delamar Mine, Lincoln County, Nevada, USA. *The Canadian Mineralogist*, **60**, 805–814.

Khidhirbrahmendra, V., Basha, S.J., Avinash, M. and Ravikumar, R.V.S.S.N. (2019) Investigations of VO^{2+} doped $SrZn_2(PO_4)_2$ nanophosphors by solution combustion synthesis. *Journal of Alloys and Compounds*, **787**, 276–283. Elsevier B.V.

Khoury, H.N., Sokol, E. V., Kokh, S.N., Seryotkin, Y. V., Nigmatulina, E.N., Goryainov, S. V., Belogub, E. V. and Clark, I.D. (2016) Tululite, $Ca_{14}(Fe^{3+},Al)(Al,Zn,Fe^{3+},Si,P,Mn,Mg)_{15}O_{36}$: a new Ca zincate-aluminate from combustion metamorphic marbles, central Jordan. *Mineralogy and Petrology*, **110**, 125–140.

Kim, A.A., Zayakina, N. V and Makhotko, V.F. (1990) Kuksite $Pb_3Zn_3TeO_6(PO_4)_2$ and cheremnykhite $Pb_3Zn_3TeO_6(VO_4)_2$ - new tellurates from the Kuranakh gold deposit (Central Aldan, southern Yakutia). *Zapiski Vsesoyuznogo Mineralogicheskogo Obshchestva*, **119**,

https://doi.org/10.1180/mgm.2025.10187 Published online by Cambridge University Press

50–57 [in Russian].

Knibbe, J. (2018) Mercury. PhD dissertation, Vrije Universiteit, Amsterdam.

Kondratieva, L.A., Anisimova, G.S. and Kardashevskaia, V.N. (2021) Types of tellurium mineralization of gold deposits of the aldan shield (Southern yakutia, russia). *Minerals*, **11**.

Krause, W., Effenberger, H., Bernhardt, H.-J. and Medenbach, O. (2008) Skorpionite, $Ca_3Zn_2(PO_4)_2CO_3(OH)_2H_2O$, a new mineral from Namibia: description and crystal structure. *European Journal of Mineralogy*, **20**, 271–280.

Krivovichev, S. V. (2020) Feldspar polymorphs: diversity, complexity, stability. *Zapiski Rossiiskogo Mineralogicheskogo Obshchestva*, **149**, 16–66.

Krivovichev, S.V., Shcherbakova, E.P. and Nishanbaev, T.P. (2012) The crystal structure of svyatoslavite and evolution of complexity during crystallization of a $CaAl_2Si_2O_8$ melt: A structural automata description. *Canadian Mineralogist*, **50**, 585–592.

Li, G., Sun, N., Shen, H., Xue, Y., Hao, J. and de Fourestier, J. (2023) Dongchuanite, a new phosphate mineral with a new structure, from Dongchuan copper mine, Yunnan Province, China. *Mineralogical Magazine*, **87**, 611–618. Cambridge University Press.

Li, P., Wang, Z., Yang, Z. and Guo, Q. (2014) Luminescent properties of $SrZn_2(PO_4)_2$:$Tb^{3+}$and its luminescence improvement by incorporating A^+(A=Li, Na, and K). *Journal of Solid State Chemistry*, **220**, 227–231. Elsevier.

Lindbloom, J.T., Gibbs, G.V., Ribbe, P.H. (1974) The crystal structure of hurlbutite: A comparison with danburite and anorthite. *American Mineralogist*, **59**, 1267-1271.

Lucas, F., Elfakir, A., Wallez, G., Quarton, M. and Lagache, M. (1998) Synthesis and rietveld refinement of new phosphate and arsenate analogues of paracelsian. *Canadian Mineralogist*, **36**, 1045–1051.

https://doi.org/10.1180/mgm.2025.10187 Published online by Cambridge University Press

Mill', B. V. (2009a) New compounds $A^{3+}Te^{6+}M_3^{3+}X_2^{5+}O_{14}$(A = Na, K; M = Ga, Al, Fe; X = P, As, V) with the $Ca_3Ga_2Ge_4O_{14}$ structure. *Russian Journal of Inorganic Chemistry*, **54**, 1355–1357.

Mill', B. V. (2009b) Synthesis of dugganite $Pb_3TeZn_3As_2O_{14}$ and its analogues. *Russian Journal of Inorganic Chemistry*, **54**, 1205–1209.

Mills, S.J., Kampf, A.R., Kolitsch, U., Housley, R.M. and Raudsepp, M. (2010) The crystal chemistry and crystal structure of kuksite, $PbM_3Zn_3Te^{6+}P_2O_{14}$, and a note on the crystal structure of yafsoanite, $(Ca,Pb)_3Zn(TeO_6)_2$. *American Mineralogist*, **95**, 933–938.

Moore, P.B. and Ito, J. (1980) Jungit und Matulait: Zwei neue taflige Phosphat-Mineralien (Jungite and matualite: Two new tabular phosphate minerals). *Der Aufschluss*, **31**, 55-61 [in German].

Mugnaioli, E., Xiong, F., Xu, X., Gemmi, M., Wirth, R., Yang, J. and Grew, E.S. (2022) Wodegongjieite, ideally $KCa_3(Al_7Si_9)O_{32}$, a new sheet silicate isostructural with the feldspar polymorph kokchetavite, $KAlSi_3O_8$. *Mineralogical Magazine*, **86**, 975-987

Pan, X., Wen, M., He, G., Li, H. and Jia, D. (2017) Syntheses, structures and properties of metal phosphates $Pb_2Mg(PO_4)_2$, $Pb_4Zn_8(PO_4)_8$ and α-$BaZn_2(PO_4)_2$. *Dalton Transactions*, **46**, 16034–16040.

Pautov, L.A., Agakhanov, A.A., Sokolova, E. and Hawthorne, F.C. (2004) Maleevite, $BaB_2Si_2O_8$, and pekovite, $SrB_2Si_2O_8$, new mineral species from the Dara-i-Pioz alkaline massif, northern Tajikistan: Description and crystal structure. *Canadian Mineralogist*, **42**, 107–119.

Pekov, I. V., Kulikova, I.M., Kabalov, Y.K. and Eletskaya, O. V. Chukanov, N. V. Menshikov, Y. P. Khomyakov, A.P. (1996) Belovite-(La) $Sr_3Na(La,Ce)[PO_4]_3(F,OH)$ – a new rare earth mineral in the apatite group. *Zapiski Vserossijskogo Mineralogicheskogo Obshchestva*, **125**,

https://doi.org/10.1180/mgm.2025.10187 Published online by Cambridge University Press

101–109 [in Russian].

Pekov, I.V. (2005) Genetic mineralogy and crystal chemistry of rare elements in high-alkaline postmagmatic system. PhD dissertation, Moscow State University, Moscow [in Russian].

Pekov, I.V., Chukanov, N.V., Kulikova, I.M., Zubkova, N.V., Krotova, O.D. and Sorokina, N.I. Pushcharovsky, D.Y. (2004) A new mineral bario-olgite and its crystal structure. *Zapiski VMO*, **133**, 41-49 [in Russian].

Phillips, M.W., Gibbs, G.V. and Ribbe, P.H. (1974) The crystal structure of danburite: A comparison with anorthite, albite, reedmergnerite. *American Mineralogist*, **59**, 79–85.

Ralph, J., Von Bargen, D., Martynov, P., Zhang, J., Que, X., Prabhu, A., Morrison, S.M., Li, W., Chen, W. and Ma, X. (2025) Mindat.org: The open access mineralogy database to accelerate data-intensive geoscience research. *American Mineralogist*, **110**, 833–844.

Rao, C., Hatert, F., Wang, R.C., Gu, X.P., Dal Bo, F. and Dong, C.W. (2015) Minjiangite, $BaBe_2(PO_4)_2$, a new mineral from Nanping No. 31 pegmatite, Fujian Province, southeastern China. *Mineralogical Magazine*, **79**, 1195–1202.

Rao, C., Wang, R., Hatert, F., Gu, X., Ottolini, L., Hu, H., Dong, C., Dal Bo, F. and Baijot, M. (2014) Strontiohurlbutite, $SrBe_2(PO_4)_2$, a new mineral from Nanping No. 31 pegmatite, Fujian Province, Southeastern China. *American Mineralogist*, **99**, 494–499.

Ribbe, P.H. (1983) The chemistry, structure, and nomenclature of feldspars. Pp. 1–20 in: *Volume 2: Feldspar Mineralogy* (P.H. Ribbe, editor). Mineralogical Society of America, Washington DC.

Robinson, G.W., Grice, J.D. and Velthuizen, J. Van. (1985) Ehrleite, a new calcium beryllium zinc phosphate hydrate from the Tip Top Pegmatite, Custer, South Dakota. *The Canadian Mineralogist*, **23**, 507–510.

Sarver, J.F., Hoffman, M. V. and Hummel, F.A. (1961) Phase Equilibria and Tin-Activated

https://doi.org/10.1180/mgm.2025.10187 Published online by Cambridge University Press

Luminescence in Strontium Orthophosphate Systems. *Journal of The Electrochemical Society*, **108**, 1103.

Shannon, R.D. (1976) Revised effective ionic radii and systematic studies of interatomic distances in halides and chalcogenides. *Acta Crystallographica*, **A32**, 751–767.

Shepard, C.U. (1839) Notice of danburite, a new mineral species. *American Journal of Science and Arts*, **35**, 137–139.

Silvio, F., Lorenzon, S., Borriello, R., Borghini, A., Wirth, R., Schreiber, A., Fuchs, R., O'Brien, P.J., Grew, E.S. and Mugnaioli, E. (2025) Pfaffenbergite, $KNa_3(Al_4Si_{12})O_{32}$, a polymorph of sodic feldspar isostructural with kokchetavite and wodegongjieite, found in crystallized melt inclusions in metamorphic garnet. *American Mineralogist,* doi: https://doi.org/10.2138/am-2025-9750

Smith, J.V. (1953) The crystal structure of paracelsian, $BaAl_2Si_2O_8$. *Acta Crystallographica,* **6**, 613-620.

Smith, J. V. and Brown, W.L. (1988) *Feldspar Minerals. Volume 1 Crystal Structures, Physical, Chemical, and Microtextural Properties*. P. in.: Springer Verlag, Berlin Heidelberg, 828 pp.

Sokol, E. V., Kokh, S.N., Seryotkin, Y. V., Deviatiiarova, A.S., Goryainov, S. V., Sharygin, V. V., Khoury, H.N., Karmanov, N.S., Danilovsky, V.A. and Artemyev, D.A. (2020) Ultrahigh-temperature sphalerite from Zn-Cd-Se-rich combustion metamorphic marbles, daba complex, central Jordan: Paragenesis, chemistry, and structure. *Minerals*, **10**, 1–47.

Strunz, H. (1948) Scholzite, a new mineral (Scholzit, eine neue Mineralar). *Fortschr. Mineral.*, **27**, 31-31 [in German].

Strunz, H. and Tennyson, C. (1956) Kristallographie von Scholzit, $CaZn_2[PO_4]_2{\cdot}2H_2O$ (Crystallography of Scholzite, $CaZn_2[PO_4]_2{\cdot}2H_2O$). *Zeitschrift für Kristallographie*, **107**, 318-324 [in German].

https://doi.org/10.1180/mgm.2025.10187 Published online by Cambridge University Press

Sturman, B.D., Rouse, R.C. and Dunn, P.J. (1981) Parascholzite, a new mineral from Hagendorf, Bavaria, and its relationship to scholzite. *American Mineralogist*, **66**, 843–851.

Sugiyama, K. and Takéuchi, Y. (1985) Unusual thermal expansion of a B-O bond in the structure of danburite $CaB_2Si_2O_8$. *Zeitschrift fur Kristallographie - New Crystal Structures*, **173**, 293–304.

Sun, N., Li, G., Xue, Y., Shen, H. and Hao, J. (2021) Cuprodongchuanite, IMA 2021-065. CNMNC Newsletter 63. *Mineralogical Magazine*, **85**.

Sun, N., Grey, I.E., Li, G., Rewitzer, C., Xue, Y., Mumme, W.G., Shen, H., Hao, J., MacRae, C.M., Riboldi-Tunnicliffe, A., Boer, S., Williams, T. and Kampf, A.R. (2024a) The new mineral cuprozheshengite, $Pb_4CuZn_2(AsO_4)_2(PO_4)_2(OH)_2$, from Yunnan, China, with site-selective As-P substitution. *American Mineralogist*, **109**, 1248–1257.

Sun, N., Li, G., Xue, Y., Shen, H. and Hao, J. (2024b) Zheshengite, $Pb_4ZnZn_2(AsO_4)_2(PO_4)_2(OH)_2$: A New Mineral of the Dongchuanite Group and the Influence of As–P Isomorphic Substitution on Unit-Cell Parameters of Dongchuanite Group Minerals. *Minerals*, **14**.

Taxer, K. (1975) Structural Investigations on Scholzite. *American Mineralogist*, **60**, 1019–1022.

Taxer, K. and Bartl, H. (1997) Die „geordnete gemittelte" kristallstruktur von parascholzit. Zur dimorphie von $CaZn_2(PO_4)_2 \cdot 2H_2O$, parascholzit – scholzit. *Zeitschrift für Kristallographie*, **212**, 197-202 [in German].

Tobase, T., Yoshiasa, A., Jinnouchi, S., Kitahara, G., Hongu, H., Tokuda, M., Okube, M. and Sugiyama, K. (2019) Crystal structure, large distortion of the Zn tetrahedron, and statistical displacement of water molecules in skorpionite. *Journal of Mineralogical and Petrological Sciences*, **114**, 178–188.

Toda, A., Androsch, R. and Schick, C. (2021) Melting kinetics of superheated polymer crystals

https://doi.org/10.1180/mgm.2025.10187 Published online by Cambridge University Press

examined by isothermal and nonisothermal fast scanning calorimetry. *Macromolecules*, **54**, 8770–8779.

Tschauner, O. and Mam C. (2017) Stofflerite, IMA 2017-062. CNMNC Newsletter No. 39, October 2017. *Mineralogical Magazine*, **81,** 1285.

Wainwright, J.E. and Starkey, J. (1971) A refinement of the structure of anorthite. *Z. Kristallogr.*, **133**, 75–84.

Wang, Z., Wang, Q., Liu, Q., Suthirakun, S., Kaewraung, W., Jiang, P., Zhao, H., Xin, X. and Subramanian, M.A. (2024) Application and properties of Co^{2+}-doped $BaAl_2Si_2O_8$ blue pigments in glazes. *CS Applied Optical Materials*, **2**, 313–322.

Wiebcke, M. (2002) $[Zn_3(HPO_4)_4](NMe_4)2$: a zincophosphate containing interruptions of isolated hydrogen-bonding $[H–O(P)]_4$ groupings within a novel three-dimensional four-connected framework. *Journal of Materials Chemistry*, **12**, 421–425.

Wood, J.A., Dickey, J.S., Marvin, U.B. and Powell, B.N. (1970) Lunar anorthosites. *Science*, **167**, 602–604.

Xu, Y., Zhang, K. and Chang, C. (2020) Effects of Bi^{3+} co-doping on structure and luminescence of $SrZn_2(PO_4)_2$-based phosphor. *Journal of Materials Science: Materials in Electronics*, **31**, 10072–10077. Springer US.

Yakovenchuk, V.N., Pakhomovsky, Y.A., Konopleva, N.G., Panikorovskii, T.L., Bazai, A., Mikhailova, J.A., Bocharov, V.N., Ivanyuk, G.Y. and Krivovichev, S. V. (2018) Batagayite, $CaZn_2(Zn,Cu)_6(PO_4)_4(PO_3OH)_3·12H_2O$, a new phosphate mineral from Këster tin deposit (Yakutia, Russia): occurrence and crystal structure. *Mineralogy and Petrology*, **112**, 591–601. Springer Vienna.

Yakubovich, O. V., Massa, W., Liferovich, R.P., Gavrilenko, P.G., Bogdanova, A.N. and Tuisku, P. (2003) Hillite, a new member of the fairfieldite group: its description and crystal

https://doi.org/10.1180/mgm.2025.10187 Published online by Cambridge University Press

structure. *Canadian Mineralogist*, **41**, 981–988.

Yang, H., Gibbs, R.B., Schwenk, C., Xie, X., Gu, X., Downs, R.T. and Evans, S.H. (2021) Liudongshengite, $Zn_4Cr_2(OH)_{12}(CO_3)\cdot 3H_2O$, a new mineral of the hydrotalcite supergroup, from the 79 mine, Gila County, Arizona, USA. *The Canadian Mineralogist*, **59**, 763–769.

Yang, W.J. and Chen, T.M. (2006) White-light generation and energy transfer in $SrZn_2(PO_4)_2$: Eu,Mn phosphor for ultraviolet light-emitting diodes. *Applied Physics Letters*, **88**, 2–5.

Yi, L., Zhou, L., Gong, F., Lan, Y., Tong, Z. and Sun, J. (2010) Preparation of $SrZn_2(PO_4)_2$: Eu^{2+}, Mn^{2+} phosphor and its photoluminescent properties. *Materials Science and Engineering: B*, **172**, 132–135.

Yuan, J.L., Zeng, X.Y., Zhao, J.T., Zhang, Z.J., Chen, H.H. and Zhang, G. Bin. (2007) Rietveld refinement and photoluminescent properties of a new blue-emitting material: Eu^{2+} activated SrZnP2O7. *Journal of Solid State Chemistry*, **180**, 3310–3316.

Zolensky, M.E., Zega, T.J., Yano, H., Wirick, S., Westphal, A.J., Weisberg, M.K., Weber, I., Warren, J.L., Velbel, M.A., Tsuchiyama, A., Tsou, P., Toppani, A., Tomioka, N., Tomeoka, K., Teslich, N., Taheri, M., Susini, J., Stroud, R., Stephan, T., Stadermann, F.J., Snead, C.J., Simon, S.B., Simionovici, A., See, T.H., Robert, F., Rietmeijer, F.J.M., Rao, W., Perronnet, M.C., Papanastassiou, D.A., Okudaira, K., Ohsumi, K., Ohnishi, I., Nakamura-Messenger, K., Nakamura, T., Mostefaoui, S., Mikouchi, T., Meibom, A., Matrajt, G., Marcus, M.A., Leroux, H., Lemelle, L., Le, L., Lanzirotti, A., Langenhorst, F., Krot, A.N., Keller, L.P., Kearsley, A.T., Joswiak, D., Jacob, D., Ishii, H., Harvey, R., Hagiya, K., Grossman, L., Grossman, J.H., Graham, G.A., Gounalle, M., Gillet, P., Genge, M.J., Flynn, G., Ferroir, T., Fallon, S., Ebel, D.S., Dai, Z.R., Cordier, P., Clark, B., Chi, M., Butterworth, A.L., Brownlee, D.E., Bridges, J.C., Brennan, S., Brearley, A., Bradley, J.P., Bleuet, P., Bland, P.A. and Bastien, R. (2006) Mineralogy and petrology of comet 81P/wild 2 nucleus samples. *Science*, **314**, 1735–1739.

https://doi.org/10.1180/mgm.2025.10187 Published online by Cambridge University Press

Zolotarev, A.A., Krivovichev, S.V., Panikorovskii, T.L., Gurzhiy, V.V., Bocharov, V.N. and Rassomakhin, M.A. (2019) Dmisteinbergite, $CaAl_2Si_2O_8$, a metastable polymorph of anorthite: crystal-structure and Raman spectroscopic study of the holotype specimen. *Minerals*, **9**, 570.

Table 1. Crystal data and structure refinement details of triclinic β-$SrZn_2P_2O_7$.

Crystal system	Triclinic
Space group, *Z*	$P\bar{1}$, 2
a (Å)	5.0109(8)
b (Å)	8.6202(13)
c (Å)	9.7527(15)
α (deg.)	118.088(3)
β (deg.)	74.622(6)
γ (deg.)	87.525(6)°
V (Å^3)	351.29(10)
Diffractometer	Rigaku Ultima IV
Radiation	Cu$K\alpha_{1+2}$
2Θ range (degrees)	5–100
Number of reflections	722
R_p %*	4.79
R_{wp} %*	6.47
R_{exp} %*	1.75
R_B %*	3.38
GOF	3.69
Program	Topas 5.0 (Bruker, 2014)
Starting model	$SrCo_2P_2O_8$ (El Bali *et al.*, 1993)
Impurity phase	3.19 wt. % of Trigonal (?) $SrZn_2P_2O_7$ (Czaya, 1972)

*

$$R_p = \frac{\sum |Y_{o,m} - Y_{c,m}|}{\sum Y_{o,m}}$$

$$R_{wp} = \sqrt{\frac{\sum w_m (Y_{o,m} - Y_{c,m})^2}{\sum w_m {Y_{o,m}}^2}}$$

$$R_{exp} = \sqrt{\frac{M - P}{\sum w_m {Y_{o,m}}^2}}$$

$$R_B = \frac{\sum |I_{o',k} - I_{c,k}|}{\sum I_{o',k}}$$

https://doi.org/10.1180/mgm.2025.10187 Published online by Cambridge University Press

Table 2. Selected bond lengths of triclinic β-$SrZn_2P_2O_7$

Bond	Bond length (Å)	Bond	Bond length (Å)	Bond	Bond length (Å)
Sr1-O7	2.38(5)	Zn1-O6	1.81(5)	P1-O3	1.50(4)
O3	2.60(5)	O4	2.04(5)	O2	1.54(6)
O2	2.63(7)	O4	2.13(4)	O4	1.53(5)
O3	2.71(5)	O5	2.23(5)	O1	1.54(6)
O1	2.77(4)	O7	2.77(4)	**<P1-O>**	**1.53**
O7	2.79(4)	**<Zn1-O>** ^{IV}	**2.05**		
O6	2.80(4)	**<Zn1-O>** ^{V}	**2.19**	P2-O7	1.51(5)
O8	2.93(4)			O6	1.52(5)
<Sr-O>	**2.70**	Zn2-O8	1.71(5)	O5	1.55(5)
		O1	1.77(5)	O8	1.56(6)
		O2	1.94(6)	**<P2-O>**	**1.54**
		O5	2.02(6)		
		O3	2.98(6)		
		<Zn2-O> ^{IV}	**1.86**		
		<Zn2-O> ^{V}	**2.08**		

Table 3. Crystallographic information of the compounds isostructural to β-$SrZn_2P_2O_8$

Compound	**β-$SrZn_2P_2O_8$**	**$SrCo_2P_2O_8$**	**α-$CaZn_2P_2O_8$**
Space group	$P\bar{1}$	$P\bar{1}$	$P\bar{1}$
***a*, Å**	5.0109(8)	5.014(2)	4.960(2)
***b*, Å**	8.6202(13)	8.639(4)	8.418(4)
***c*, Å**	9.7527(15)	9.691(1)	8.940(4)
α, °	118.088(3)	118.04(3)	113.75(4)
β, °	74.622(6)	75.09(4)	102.45(5)
γ, °	87.525(6)°	86.90(4)	94.20(6)
***V*, Å^3**	351.29(10)	350.41	328.23
Reference	This work	El Bali *et al.*, 1993	Jakeman and Cheetham, 1988

https://doi.org/10.1180/mgm.2025.10187 Published online by Cambridge University Press

Table 4. Thermal expansion coefficients (TECs) ($\times 10^6$ °C^{-1}) of $SrZn_2P_2O_8$ along the principle axes of the thermal expansion tensor and along the crystallographic axes

Compound (space group)	ΔT, °C	α_{11}	α_{22}	α_{33}	$\mu_{(\alpha 33 \wedge c)}$	α_a	α_b	α_c	α_α	α_β	α_γ	α_V	α_{max} / α_{min}
$SrZn_2P_2O_8$ ($P2_1/c$)	30–900	14.3(1)	2.9(1)	7.8(2)	44.6(9)	10.84(1)	2.9(1)	11.0(2)	–	–3.98(9)	–	25.0(2)	4.9
$SrZn_2P_2O_8$ ($P\bar{1}$)	30–600	10.2(2)	2.5(2)	14.1(3)	14.3(2)	8.7(2)	5.3(2)	13.6(3)	0.86(8)	–3.7(2)	5.6(2)	26.7(4)	5.6

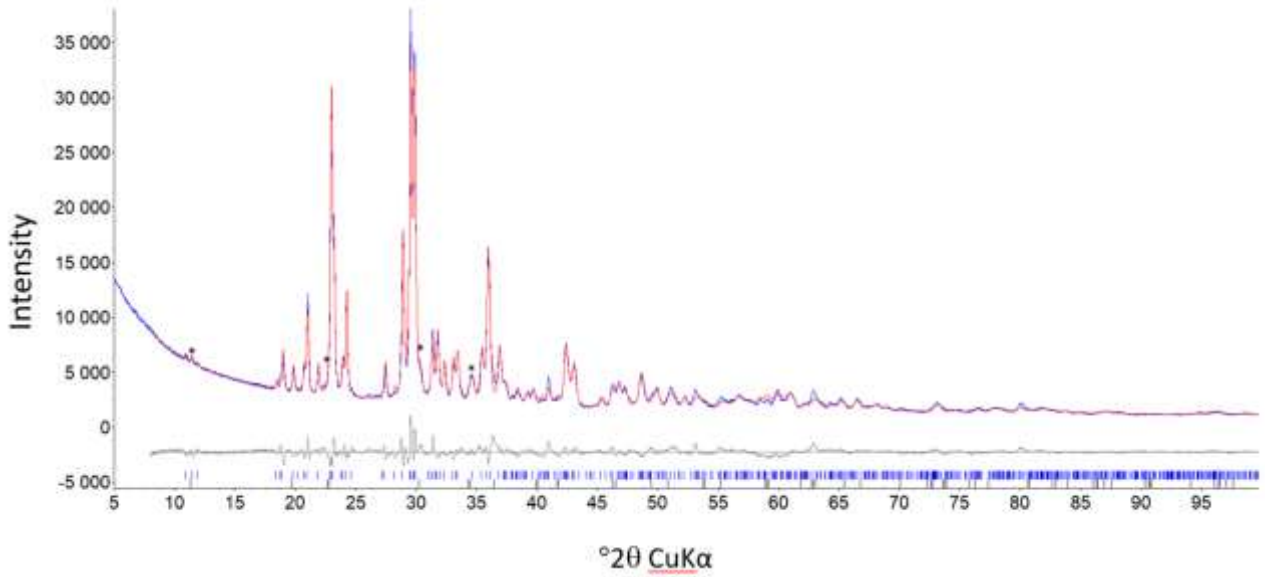

Figure 1. Final Rietveld plot of triclinic β-$SrZn_2P_2O_7$. Blue line shows experimental PXRD data, red line corresponds to the calculated XRD data, grey line is the difference between the measured and calculated XRD patterns. Peak positions of triclinic β-$SrZn_2P_2O_7$ are shown in the lowest part of the figure in blue. Black ticks correspond to the admixture of about 3.1 wt. % of presumably trigonal $SrZnP_2O_7$; its most intensive peaks are marked by asterisks.

https://doi.org/10.1180/mgm.2025.10187 Published online by Cambridge University Press

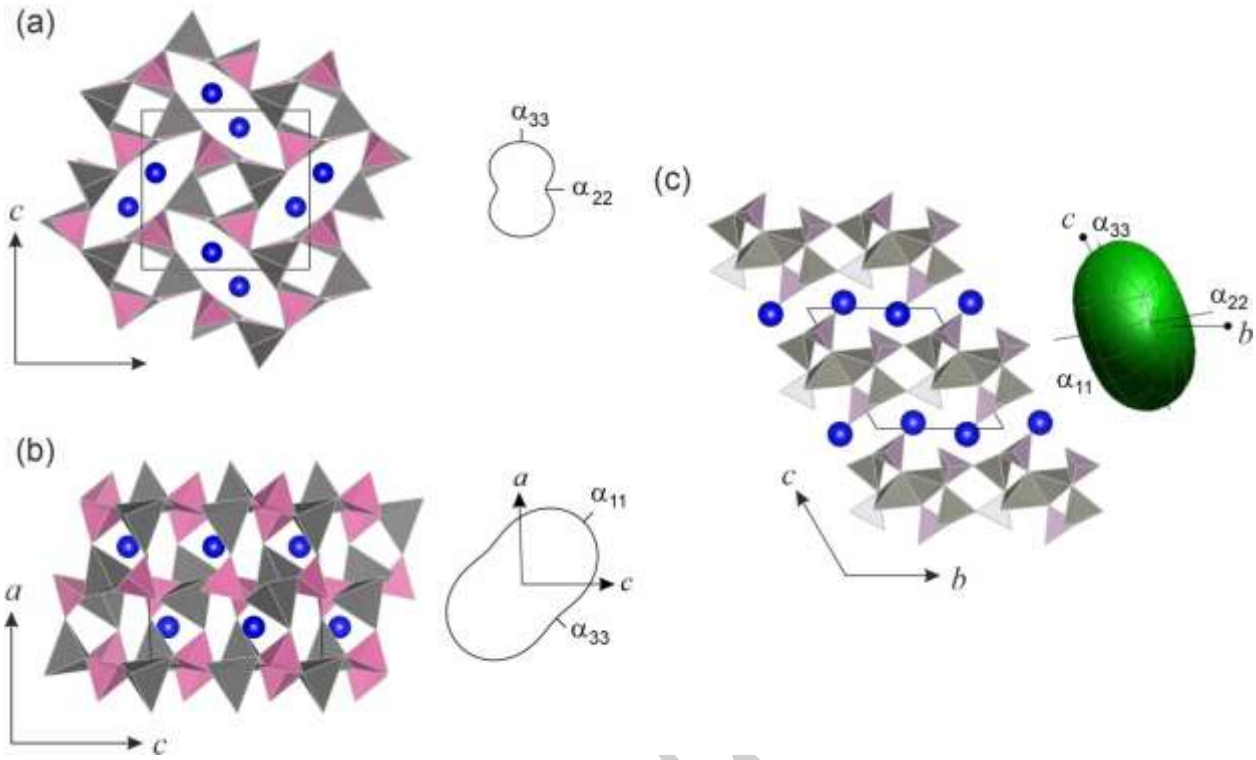

Figure 2. Crystal structures of α- (a, b) and β-$SrZn_2P_2O_8$ (c) with the section of thermal deformations. PO_4 and ZnO_4 tetrahedra are given in purple and grey, respectively. Sr atoms are presented as blue spheres.

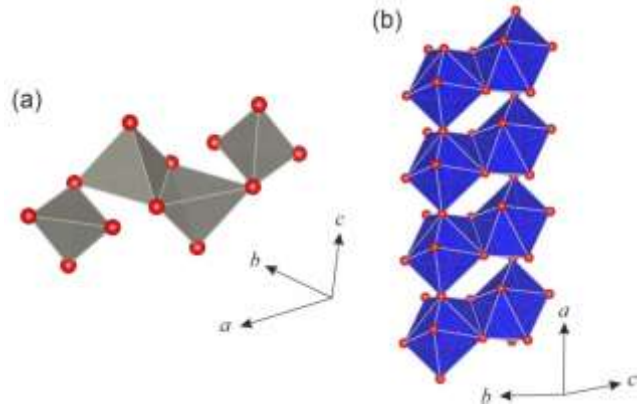

Figure 3. Fragments of β-$SrZn_2P_2O_8$: (a) Zn_4O_{12} structural units; (b) chain of SrO_8 polyhedra. Grey and blue polyhedra show ZnO_n (n = 4, 5) and SrO_8 polyhedra, respectively; red spheres indicate oxygen atoms.

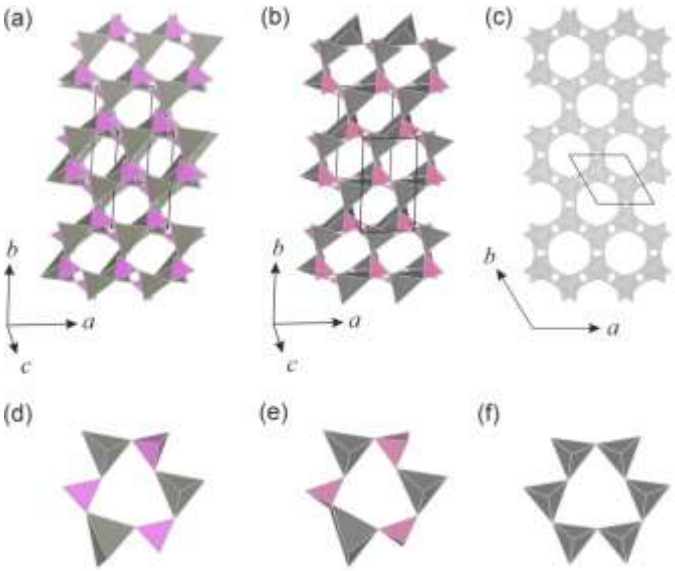

Figure 4. Double layers and six-membered rings in hexacelsian-type compounds: of β-$SrZn_2P_2O_8$ (a, d), α-$CaZn_2P_2O_8$ (b, e) (Jakeman and Cheetham, 1988) and β-dmisteinbergite (c, f) (Gorelova *et al.*, 2023b). PO_4 tetrahedra and ZnO_n (n = 4, 5) polyhedra in crystal structures of β-$SrZn_2P_2O_8$ and α-$CaZn_2P_2O_8$ are given in purple and grey, respectively. Grey tetrahedra in β-dmisteinbergite show mixed TO_4 (T = Si, Al) tetrahedra.

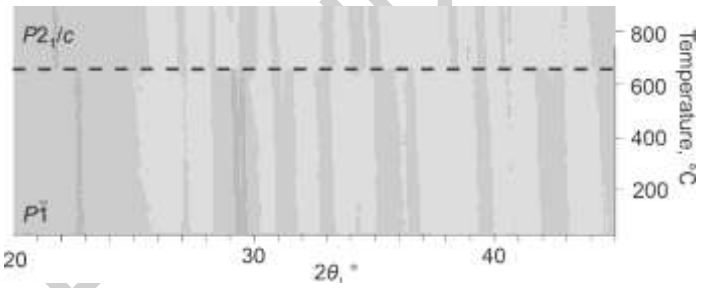

Figure 5. The evolution of the PXRD patterns of β-$SrZn_2P_2O_8$ in the range 30–900 °C.

https://doi.org/10.1180/mgm.2025.10187 Published online by Cambridge University Press

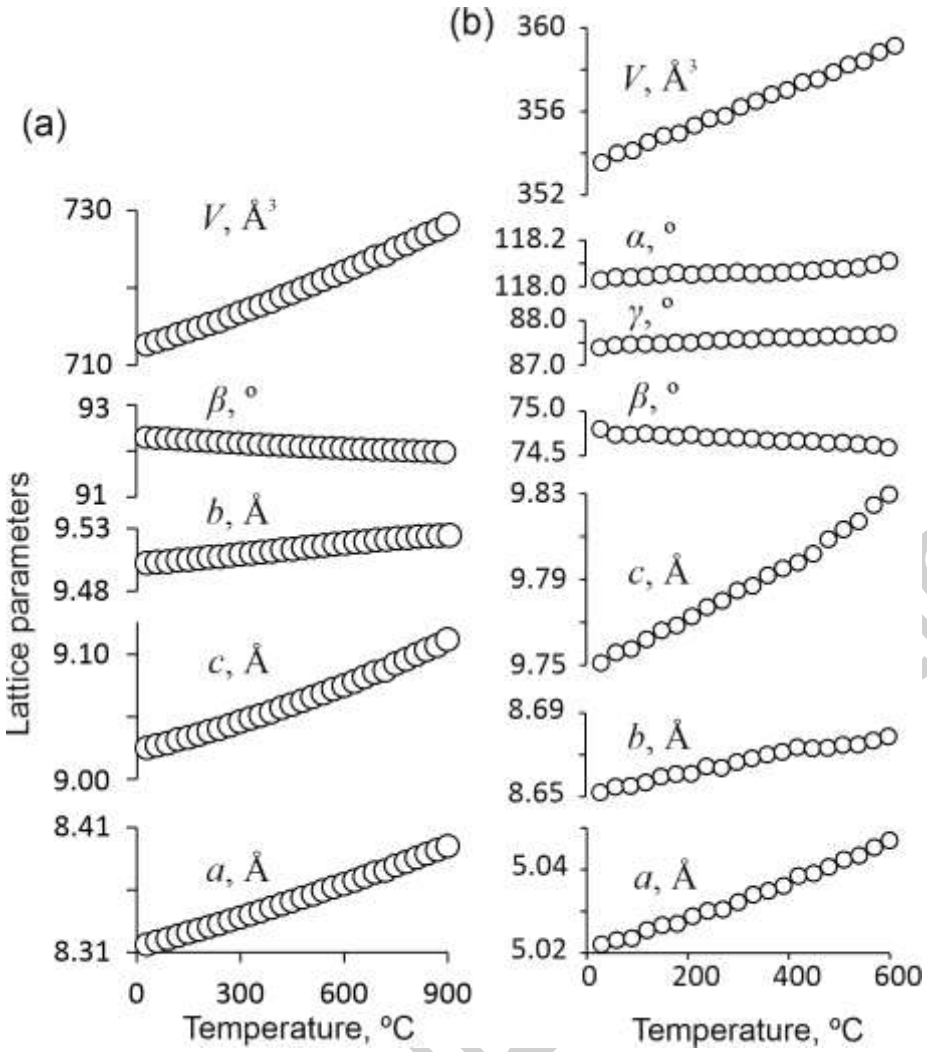

Figure 6. Unit-cell parameters of α-$SrZn_2P_2O_8$ (a) and β-$SrZn_2P_2O_8$ (b) at different temperatures. Errors are smaller than symbols.

https://doi.org/10.1180/mgm.2025.10187 Published online by Cambridge University Press